# Feasibility studies of two-dimensional edge turbulence measurements by laser induced fluorescence

C. H. Skinner and S. J. Zweben
*Princeton University, Plasma Physics Laboratory, PO Box 451, Princeton, New Jersey 08543*

F. M. Levinton
*Fusion Physics and Technology, Torrance, California*

J. McChesney
*25518 Hardy Place, Stevens Ranch, California*

(Presented on 10 June 1998)

Edge turbulence is a key factor in the performance of fusion devices but is not well understood even after many years of research. We assess the feasibility of using laser induced fluorescence to obtain two-dimensional images of turbulent structures in the plasma. Based on theoretical expectations of density fluctuations arising from turbulence and calculations of level populations in He-like and noble gas ions we show that high signal/noise ratios ($S/N>100$) may be expected for experimental conditions in the magnetic reconnection experiment and on the National Spherical Torus Experiment at PPPL. Schemes include exciting the ion emission lines such as B IV 282.3 nm or Kr II 441.8 nm by a tunable laser. © *1999 American Institute of Physics.*
[S0034-6748(99)65901-9]

## I. INTRODUCTION

Turbulence is a key factor limiting the performance of fusion devices and other plasma related systems. Edge turbulence determines the boundary values of the plasma density and temperature, which in turn determines the internal gradients and controls global plasma transport. The structure of the turbulence in the cold outer edge has been determined by local probe measurements, but these are not usable in the hotter plasma past the separatrix. Knowledge of the local structure of the edge turbulence near the separatrix would be extremely useful in clarifying our understanding of the physics and empirical scaling of the $L-H$ transition, a key factor in the ignition scenario of the International Thermonuclear Experimental Reactor (ITER) or other fusion reactor designs. Plasma devices such as reversed field pinches, stellarators, and other innovative concepts would also benefit. In this article we explore the feasibility of using laser induced fluorescence (LIF) to provide the first experimental measurements of the two-dimensional (2D) spatial structure of density and flow of plasma turbulence in magnetically confined plasmas.

Existing diagnostic instrumentation for the study of structure and magnitude of micro turbulent processes has been recently reviewed.[1] Much work has been done however, even broad issues such as whether the transport depends on the size of the device or on the ion gyroradius, or whether the turbulence induced transport is mainly electrostatic or magnetic have proven difficult to resolve. LIF techniques at a single point or along a chord in space have been successfully applied to measurements of hydrogen density, velocity, and magnetic field measurements in high temperature plasmas.[2] For example, radial profiles of density and velocity of atomic deuterium in the boundary of TEXTOR 94 have been measured using a Lyman-alpha laser.[3] Planar laser fluorescence has been applied to measurements of the velocity flow of coherent drift waves in argon plasmas in the Encore Tokamak.[4] Lithium beam emission spectroscopy has been applied to investigate edge plasma density and fluctuations.[5] In the field of fluid mechanics, 2D visualization using planar laser induced fluorescence (PLIF) has been a critical tool in understanding fluid flows and turbulence.[6] PLIF visualization of the chemistry and flow patterns has been applied to problems in combustion research.[7]

In this article the space and time scales of turbulence in plasmas in the Magnetic Reconnection Experiment[8] (MRX) and on the National Spherical Torus Experiment (NSTX)[9] at PPPL are estimated. The application of PLIF techniques to visualize the density and flow turbulence using ion transitions in both He-like ions (Li II, B IV, and C V) and noble gas ions Ar II and Kr II is considered. Level populations are calculated from collisional radiative codes and signal/noise levels for specific experimental conditions are estimated. Several cases with signal/noise ratios over 100 are identified.

## II. EXPECTED TURBULENCE CHARACTERISTICS IN MRX AND NSTX

A universal feature of Tokamak plasmas is the presence of density fluctuations near the plasma edge with an amplitude $\tilde{n}/n \approx 0.1-0.5$.[10] Results from various turbulence diagnostics on tokamaks and stellarators,[1,11,12] e.g., Langmuir probes, microwave scattering and reflectometry, heavy ion beam probes, and on the associated theory used to interpret these results enable us to estimate the expected turbulence characteristics of MRX and NSTX. The amplitude, space, and time scales are listed in Table I.

In NSTX, the radial region of the LIF measurement is determined by the location of the zone in which the electron

 

TABLE I. Estimated turbulence parameters for NSTX ($r/a \approx 1$) and MRX ($r/a \approx 0.5$). $L_n$ is the density gradient scale length, $\tilde{n}/n$ is the normalized density fluctuation, $v_d$ the toroidal drift velocity, $L_{\text{turb}}$ the poloidal correlation length, $\tau_{\text{turb}}$ the autocorrelation time.

| Parameter | NSTX | MRX |
|---|---|---|
| $T_e$ | 25 (eV) | 10 (eV) |
| $B$ | 2000 (G) | 300–900 (G) |
| $L_n$ | 3 cm | 5–10 cm |
| $\tilde{n}/n$ | 0.5 | 0.3–0.7 |
| $v_d$ | $4\times10^5$ cm/s | $1-3\times10^5$ cm/s |
| $L_{\text{turb}}$ | 3 cm | 5–15 cm |
| $\tau_{\text{turb}}$ | 8 $\mu$s | 10–50 $\mu$s |

temperature is $T_e \approx 10-100$ eV, where the appropriate ionic states of carbon or argon impurity ions are located. This is most likely in the outer edge region near $r/a \approx 1.0 \pm 0.1$ ($a$ is the minor radius), where the toroidal field is very low due to the low aspect ratio. The largest uncertainty here is in the density gradient scale length, which may be as short as $L_n \approx 1$ cm if there is a sharp ''*H*-mode-like'' edge, or as long as $L_n \approx 5$ cm for a soft ''*L*-mode-like'' edge dominated by Bohm diffusion. It is interesting to note that these estimated turbulence space and time scales are similar to those measured for the Macrotor tokamak[13] which had edge parameters similar to those assumed above, but an aspect ratio of $R/a \approx 2$ ($R$ is the major radius).

In MRX, the main plasma parameters and magnetic geometry are substantially different from NSTX, and it is not clear what character the drift wave turbulence will take. However, the estimates can be done using the same formalism. The radial position of the LIF measurement for MRX would be closer to the plasma center, since the central electron temperature is in the range $T_e \approx 10-20$ eV. This calculation implies that these types of drift waves in MRX would be comparable to the plasma size scale and lifetime, which would make them more similar to global modes than small-scale turbulence. However, it should be emphasized that neither the experimental nor the theoretical data is available yet to verify these estimates.

Strong drift wave turbulence, is predicted from estimates based on the ''mixing length model'' [12] $\tilde{n}/n \approx 0.5$ for NSTX and $\tilde{n}/n \approx 0.7$ for MRX. This is consistent with the measured results for the edge plasmas of tokamaks and stellarators.[11,12] The expected fluctuating radial velocity of the ions can be calculated based on the assumption that they are responding to $\tilde{E} \times B$ drifts in these fluctuations. The resulting fluctuating radial velocities are $\tilde{v}_r \approx 2\times10^5$ cm/s for both NSTX and MRX. Assuming that $T_i \approx T_e$, these velocities are about 0.1–0.2 times the thermal velocity of carbon in NSTX, but comparable to the thermal velocity of argon in MRX. Excitation of a particular velocity class by sub-Doppler LIF may enable velocity measurement to be made at the same place and time as the density fluctuation measurements, offering the potential for direct measurements of the local radial transport of ions due to turbulence.

Edge turbulence usually has much longer scale lengths parallel to the field than perpendicular to the field. The density fluctuations to be measured by LIF can be assumed to be slowly varying in the direction parallel to the main magnetic field; therefore, the laser pumping and optical sight lines can integrate over parallel lengths much larger than the perpendicular turbulence size scales. A possible experimental configuration is shown in Fig. 1.

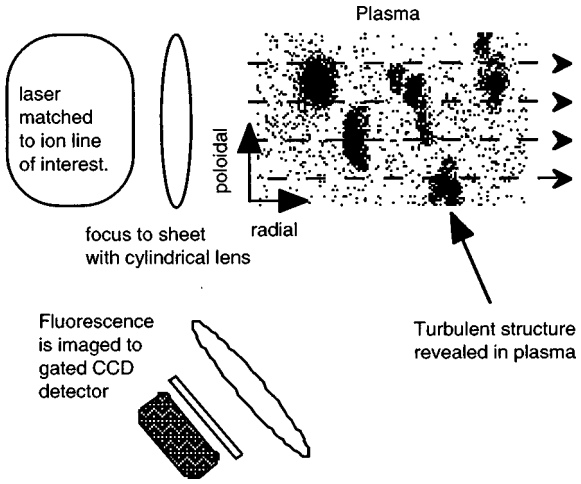


FIG. 1. Basic experimental scheme.

## III. COLLISIONAL RADIATIVE MODELING OF HE-LIKE IONS

The time dependent populations of several potential ions for LIF were calculated using collisional radiative models. For the low-$Z$ ions of helium, lithium, boron, and carbon the collisional radiative code, FLY[14] was used. This code models lithium-, helium-, and hydrogen-like species from $Z = 2-26$. Helium is an interesting candidate for LIF since it can be added to a hydrogenic plasma with no appreciable increase in radiated power losses and has a transition at a convenient wavelength, He II 468.6 nm, $n=3 \rightarrow n=4$. However, the $n=3$ and $n=4$ excited states were predicted to have similar populations, due to fast collisional transitions. Stimulated emission and absorption induced by the laser beam would not change these populations significantly and hence it would be difficult to detect fluorescence. Fortunately, more accessible transitions in the rare gases, such as Ar II, are available for LIF in this low temperature regime (see Sec. IV). These ions are also more suitable for velocity measurements because of their large mass.

Helium-like ions are attractive for LIF because they have a high lying $2s^3S$ metastable state. Table II shows the ion-

TABLE II. Candidate LIF transitions in He-like ions.

| Ion | Ionization potential | $2s^3S-2p^3P$ Wavelength |
|---|---|---|
| He I | 24.6 eV | 1,083 nm |
| Li II | 75.6 eV | 548.5 nm |
| Be III | 153 eV | 372.2 nm |
| B IV | 259 eV | 282.3 nm |
| C V | 392 eV | 227.1 nm |
| N VI | 552 eV | 190.1 nm |

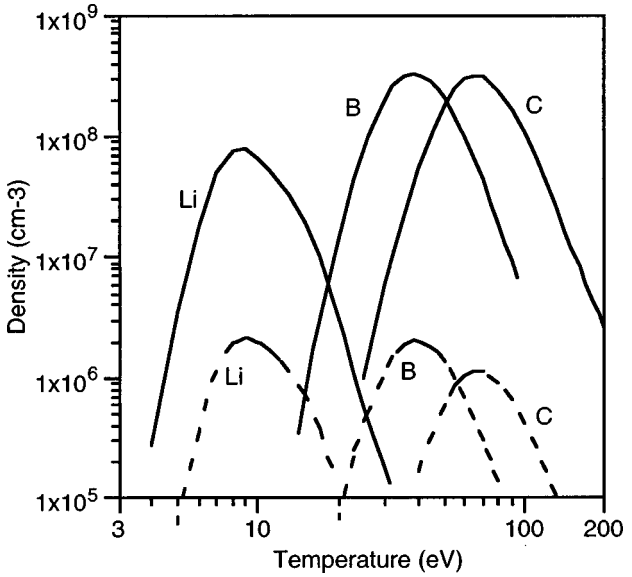


FIG. 2. Excited state populations of helium-like lithium, boron, and carbon as predicted by the FLY code. The plasma composition is 10% Li, B, or C in a background of 90% $H^+$; the electron density is $n_e = 10^{13}$ cm$^{-3}$. The upper solid curve refers to the metastable level, $2s^3S$; the lower dashed curves to the $2p^3P$ level.

ization potentials and the wavelength of the $2s^3S-2p^3P$ transition in neutral helium and some low $Z$ He-like ions. For Li II, Be III, B IV, and C V the transitions are in the 2000–6000 Å wavelength range. Beryllium presents special handling difficulties due to its toxicity and is not discussed further. The other ions can be readily introduced into plasmas. The range in ionization potential of these ions offers coverage of a range of different temperature regions of the plasma. This scheme avoids one of the difficulties of LIF with non He-like ions in higher temperature plasmas (above 10 eV) as the other ions at these temperatures mostly have strong transitions in the vacuum ultraviolet where tunable laser operation is difficult.

Figure 2 shows the FLY calculations of He-like excited state populations for steady state conditions. The high metastable population of the $2s^3S$ level and the comparatively low population of the upper level $2p^3P$ provides very favorable conditions for LIF. The excited states of He-like ions are likely to be close to equilibrium with the plasma because of the high ionization potential and correspondingly long lifetime before further ionization.

In LIF, the $2s^3s$ and $2p^3P$ levels may be approximated as a two level system excited by an intense resonant laser pulse. With a laser intensity such that stimulated emission dominates spontaneous emission the population dynamics will be dominated by absorption and stimulated emission and the populations distributed according to the level statistical weights. The $2p^3P$ population will rise on a nanosecond time scale to close to 3/4 of the combined previous $2s^3S$ and $2p^3P$ level populations. Radiative decay by the $2p^3P-1s^1S$ transition is forbidden and we expect the total $2s^3S$ and $2p^3P$ level populations to be largely maintained during the 500 ns laser pulse.

The $2p^3P$ level is split by fine structure. For example, in He-like Li II the (vacuum) wavelengths for transitions from the $2p^3P_0$, $2p^3P_1$, $2p^3P_2$ are at 548.5, 548.59, and 548.66 nm, respectively.[15] For comparison, the Doppler linewidth at 9 eV (the peak of the Li curve in Fig. 2) is 0.05 nm. These lines will also be split by the Zeeman effect by an amount, $\Delta_z = g_J \mu_B B$, where $g_J$ is the Lande $g$ factor (of order unity), $\mu_B$ the Bohr magneton, and $B$ the magnetic field. In the magnetic field of 900 G in MRX or 2 kG for NSTX this corresponds to a wavelength splitting of 0.002 and 0.004 nm, respectively, negligible compared to the Doppler width. The partially blended transitions: $2s^3S-2p^3P_1$, $2p^3P_2$ would be excited. The $2p^3P_0$ sublevel will be populated by collisional transfer, radiatively decay predominantly to the $2s^3S$ level, and be available for reexcitation. One experimental complication is that one needs an effective laser beam dump to avoid stray laser light contributing to the fluorescence signal. The fluorescence can be distinguished by its nonlinear (saturated) dependence on laser power.

The signal/noise of the fluorescence is calculated from the excited state populations (Fig. 2) within the two-level approximation. We treat a case with an electron density of $n_e = 10^{13}$ cm$^{-3}$ (typical of edge plasma conditions in MRX), with 10% of the ion density being Li, B, or C, in a background of $H^+$. We consider high throughput, $f/1.2$, collection optics. To detect the image of the LIF signal, a 10 cm $\times$10 cm area of plasma is imaged onto a gated, intensified, 512$\times$512 pixel CCD camera. For estimates of signal-to-noise it is assumed that pixels are averaged together into a reduced 30$\times$30 element array corresponding to about an area of 0.34 cm$\times$0.34 cm in the plasma. The fluorescent signal is collected from a volume element of 0.34 cm$\times$0.34 cm $\times$1.5 cm (assuming a 1.5-cm-thick planar laser beam), with background emission from a much thicker volume: 0.34 cm $\times$0.34 cm$\times$20 cm. The signal is estimated from the equation

$$S = \Delta n_2 A_{21} V_s (\Omega/4\pi) \tau \eta T,$$

where $S$ is the collected number of photoelectrons, $\Delta n_2$ is the change, relative to the ground state, in the level 2 population from laser pumping, $A_{21}$ the spontaneous transition rate between levels 2 and 1, $V_s$ the volume from which the signal is collected, $\Omega$ is the solid angle, $\tau$, the duration of the laser pulse, $\eta$ is the detector quantum efficiency, and $T$ is the interference filter transmission. There is a corresponding equation for the background signal, based on the level 2 population without laser pumping. The signal-to-noise is defined as, $S/N = S/\sqrt{S+B}$, where $S$ is the number of collected photoelectrons from the fluorescence signal and $B$ is the corresponding photoelectrons from background emission.

The signal intensity, background intensity, and signal-to-noise are shown in Table III for a laser intensity $10^3-10^4$ W/cm$^2$ (sufficient for stimulated emission to dominate spontaneous emission), laser bandwidth set to match the Doppler broadened linewidth, and pulse duration of 500 ns. The laser intensity necessary for stimulated absorption to equal the spontaneous emission rate for these transitions is 0.15, 4.2, and 12 kW/cm$^2$ for Li II, B IV, and C V, respectively. Alexandrite lasers are available that meet these requirements for the Li II and B IV cases, however they fall somewhat short at present for the C V case.

TABLE III. Signal/noise calculations for He-like ions.

| Parameter: | Li | B | C |
|---|---|---|---|
| $T_e$ (eV) | 9 | 38 | 60 |
| Laser wavelength | 548.5 nm | 282.3 nm | 227.1 nm |
| Upper state population —with laser | $6.1e+07$ | $2.5e+08$ | $2.2e+08$ |
| Upper state population —w/o laser | $2.0e+06$ | $2.0e+06$ | $1.0e+06$ |
| A value ($s^{-1}$) | $2.3e+07$ | $3.4e+07$ | $5.7e+07$ |
| Filter transmission | 50% | 30% | 10% |
| Quantum efficiency | 35% | 25% | 25% |
| Signal (photoelectrons) | $2.1e+04$ | $5.6e+04$ | $2.8e+04$ |
| Background (photoel.) | $1.0e+04$ | $5.9e+03$ | $1.7e+03$ |
| S/N | 120 | 225 | 162 |

TABLE IV. Results for Kr II and Ar II transitions. $n_1$ is the initial level, $n_2$ the level excited by the laser. $\Delta n_2/n_1$ is the change in the population ratio due to laser excitation after an initial transient. $A_{23}$ ($s^{-1}$) is the spontaneous transition probability for the fluorescent transition.

| Ion | Kr II | Ar II | Ar II | Ar II |
|---|---|---|---|---|
| $n_e$ ($cm^{-3}$) | $10^{13}$ | $10^{13}$ | $10^{13}$ | $10^{13}$ |
| Laser λ (nm) | 441.8 | 385.1 | 433.1 | 611.5 |
| Fluorescence λ (nm) | 503.4 | 392.9 | 443.0 | 460.9 |
| $n_2/n_1$ | $2.0e-04$ | $5.7e-05$ | $7.7e-05$ | $4.0e-05$ |
| $\Delta n_2/n_1$ | $8.0e-04$ | $1.8e-04$ | $2.9e-04$ | $5.0e-04$ |
| $A_{23}$ ($s^{-1}$) | $4.5e+08$ | $3.9e+07$ | $6.3e+07$ | $1.1e+08$ |
| Signal | $5.6e+06$ | $1.1e+05$ | $2.8e+05$ | $8.4e+05$ |
| Background | $1.9e+07$ | $4.5e+05$ | $9.9e+05$ | $9.0e+05$ |
| S/N | 1,100 | 140 | 250 | 640 |

Since the background light is integrated through a plasma that is thick, it is assumed that the small scale density fluctuations are averaged out. Larger scale structure may not average out completely. This would be measured separately and subtracted out to yield the fluorescent signal. This can be done with a single detector and comparing shots with and without the laser. Alternatively, a dual camera system can be used to obtain two images, very closely spaced in time, which would then be subtracted. The dual camera system or an advanced fast framing CCD systems[16] would be used to obtain information on the time dependence of fluctuations. As estimated in Sec. II the fluctuation level at the plasma edge is 30%–70%. For a measurement uncertainty of 10% of the fluctuation amplitude and a very conservative fluctuation level of 10%, then a signal-to-noise of ≈100 is required. As shown in Table III all the transitions meet this criterion.

## IV. MODELING OF NE, AR, AND KR

Several promising LIF transitions were found for neon, argon, and krypton by using the HULLAC code.[17] HULLAC is a suite of several codes that calculates the level structure and populations for ions of higher $Z$ elements. It has been used to find 90 new LIF schemes in argon.[18] Once the energy levels and rate coefficients are calculated, the population level of each state is found using a coronal model. This is a three level scheme in which the laser excites a highly populated target state to an upper level which fluoresces to a (different) lower state.

We estimate the signal/noise ratio with the same formalism as Sec. III. The fluorescence in these cases is at a different wavelength than the laser excitation which reduces the difficulty of separating the fluorescence signal from the laser light. Results for Kr II and Ar II transitions are shown in Table IV. As before, the predicted signal/noise is ample for turbulence measurements S/N>100. The availability of LIF transitions with a wide range of ionization potentials offers coverage of a wide range of plasma conditions.

Ion flows may potentially be measured by sub-Doppler laser excitation. If the S/N is sufficient, it may be possible to use a narrow band laser to excite a particular velocity class of ions. At some cost in experimental complexity, one could envisage a two laser beam system (broad and narrow band) that measured both the overall density fluctuations and the density of a particular velocity class of ions.

We conclude that visualization of turbulent structures in plasmas is feasible using laser fluorescence techniques. Based on theoretical expectations of density fluctuations arising from turbulence and calculations of level populations in He-like and noble gas ions we have shown that the signal/noise ratios expected for experimental conditions in MRX and NSTX are more than enough for turbulence measurements. LIF visualization of turbulence promises to be extremely useful in clarifying our understanding of the physics of plasma transport.

## ACKNOWLEDGMENTS

We would like to acknowledge the assistance of B. Denne with Kr and Xe structure, K. Fournier with the HULLAC calculations, R. Maingi with NSTX parameters. This work was supported by the U. S. Department of Energy Contract No. DE-FG03-97ER82384.

[1] N. Bretz, Rev. Sci. Instrum. **68**, 2927 (1997).
[2] K. Muraoka and M. Maeda, Plasma Phys. Controlled Fusion **35**, 633 (1993).
[3] Ph. Mertens and M. Silz, Nucl. Mater. **241–243**, 842 (1997).
[4] A. D. Bailey, R. A. Stern, and P. M. Bellan, Phys. Rev. Lett. **71**, 3123 (1993).
[5] D. M. Thomas, Rev. Sci. Instrum. **66**, 806 (1995); IEEE Trans. Plasma Sci. **24**, 27 (1996).
[6] R. B. Miles and W. R. Lempert, Annu. Rev. Fluid Mech. **29**, 285 (1997).
[7] R. K. Hanson, J. Quant. Spectrosc. Radiat. Transf. **40**, 343 (1998).
[8] M. Yamada *et al.*, Phys. Plasmas **4**, 1936 (1997).
[9] C. Neumeyer *et al.*, Proceedings of the 17th IEEE Symposium on Fusion Engineering (SOFE), San Diego, October 1997, Vol. 1, p. 221.
[10] C. M. Surko, Comments Plasma Phys. Control. Fusion **10**, 265 (1987).
[11] A. J. Wotton *et al.*, Phys. Fluids B **2**, 2879 (1990).
[12] P. C. Liewer, Nucl. Fusion **25**, 543 (1995).
[13] S. J. Zweben *et al.*, Phys. Rev. Lett. **42**, 1270 (1979).
[14] R. W. Lee and J. L. Larsen, J. Quant. Spectrosc. Radiat. Transf. **56**, 535 (1996).
[15] S. Bashkin and J. O. Stoner, *Atomic Energy Levels and Grotrian Diagrams* (North-Holland, Amsterdam, 1975).
[16] Princeton Scientific Instruments Inc., Monmouth Jct., NJ 08852.
[17] A. Bar-Shalom and M. Klapisch, Comput. Phys. Commun. **50**, 375 (1988).
[18] J. M. McChesney, K. I. Lippman, W. Goldstein, and K. B. Fournier, Rev. Sci. Instrum. **66**, 600 (1995).